Available online at www.sciencedirect.com
SCIENCE DIRECT
Journal of Colloid and Interface Science 285 (2005) 769–780
JOURNAL OF Colloid and Interface Science
www.elsevier.com/locate/jcis

Linear stability of a surfactant-laden annular film in a time-periodic pressure-driven flow through a capillary

Hsien-Hung Wei [a,*], David Halpern [b], James B. Grotberg [c]

[a] *Department of Chemical Engineering, National Cheng Kung University, Tainan 701, Taiwan*
[b] *Department of Mathematics, University of Alabama, Tuscaloosa, AL 35487, USA*
[c] *Department of Biomedical Engineering, University of Michigan, MI 48109, USA*

Received 4 August 2004; accepted 30 November 2004

Available online 27 January 2005

Abstract

This paper analyzes the effect of surfactant on the linear stability of an annular film in a capillary undergoing a time-periodic pressure gradient force. The annular film is thin compared to the radius of the tube. An asymptotic analysis yields a coupled set of equations with time-periodic coefficients for the perturbed fluid–fluid interface and the interfacial surfactant concentration. Wei and Rumschitzki (submitted for publication) previously showed that the interaction between a surfactant and a steady base flow could induce a more severe instability than a stationary base state. The present work demonstrates that time-periodic base flows can modify the features of the steady-flow-based instability, depending on surface tension, surfactant activity, and oscillatory frequency. For an oscillatory base flow (with zero mean), the growth rate decreases monotonically as the frequency increases. In the low-frequency limit, the growth rate approaches a maximum corresponding to the growth rate of a steady base flow having the same amplitude. In the high-frequency limit, the growth rate reaches a minimum corresponding to the growth rate in the limit of a stationary base state. The underlying mechanisms are explained in detail, and extension to other time-periodic forms is further exploited.

Keywords: Core–annular film flow; Time oscillatory; Capillary instability; Surfactant; Marangoni

1. Introduction

When two immiscible fluids are subjected to an external pressure in a cylindrical tube, they typically flow coaxially in a core–annular flow (CAF) arrangement in which one (the annular) fluid coats the wall and surrounds the other (the core) fluid (see Fig. 1). CAFs have been extensively studied and served as useful models in a variety of contexts such as lubricated pipelining [1], liquid–liquid displacement in porous media [2], secondary oil recovery [3] and pulmonary airway closure [4,5]. In most applications, the annular thickness is small compared to the tube radius. A CAF in this situation is called a core–annular film flow (CAFF). The dynamics of a CAFF are often controlled by the annular film, and usually include events of how the fluid–fluid interface evolves, depending on flow conditions and fluid properties. In some instances the interface could remain intact while in others it could become discontinuous (e.g., snap-off). This is the interfacial instability that affects the integrity of a CAFF and hence the subsequent fate of the system. It is so critical to a CAFF that one needs to properly manage it to encourage or discourage instability for desired processes. In this paper, we restrict our attention to CAFFs and relevant physics in interfacial instability.

The motivation of the present study of CAFFs arises from efforts to understand, for example, oil recovery processes and the mechanisms involved in airway closure. In these applications, flows are typically time-periodic and often contain surface-active agents such as surfactants. The role of time periodicity, surfactant, or their combination could be vital to these processes. In secondary oil recovery, it is usual

* Corresponding author.
E-mail address: hhwei@mail.ncku.edu.tw (H.-H. Wei).

0021-9797/$ – see front matter
doi:10.1016/j.jcis.2004.11.069

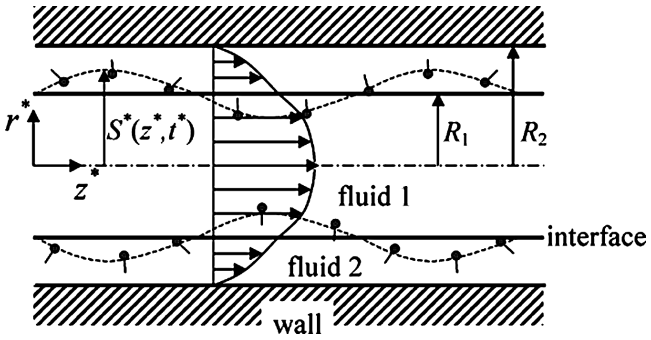

Fig. 1. Geometry of a core–annular film flow in the presence of surfactant.

to pump an immiscible fluid (e.g., water) into porous rocks to extract residual oil lodged therein. As the interfacial instability occurs due to high interfacial tensions, the wetting layer (oil) snaps and brings the nonwetting phase (water) into contact with the capillary pore wall, thereby making recovery more difficult. Adding surfactant reduces surface tension, discouraging the inception of instability and thus improving recovery efficiency. Time-oscillatory forces generated by acoustic waves could also discourage the interface from contacting the wall, and thus could provide an efficient means to displace residual oil out of porous media [6].

In the lung, air travels through a network of airways whose walls are coated by a thin fluid layer. The interfacial dynamics of such a liquid layer is critical to maintaining normal breathing. For premature infants suffering from respiratory diseases such as respiratory distress syndrome (RDS), insufficient surfactant or the surfactant deficiency could exaggerate the interfacial growth during a breathing cycle. This growth in turn blocks the pathway for air to reach alveoli, where gas exchange takes place. To prevent such a catastrophic event, one should discourage the surface-tension-induced (capillary) instability. Surfactant replacement therapy (SRT) is often a remedy for RDS. Normal procedures involve instillation of a liquid bolus into the lung as a vehicle to deliver exogenous surfactants. Such liquid often forms a liquid plug and leaves a trailing film behind or ahead of the plug. In contrast to airway closure, it is necessary to appropriately manage the formation of liquid plugs, e.g., via breathing rates, in order to efficiently deliver surfactants.

The dominant effects on the linear stability of a CAFF are capillarity and viscosity stratification. The detailed features of each effect and their combined influence have been studied thoroughly [1,7,8]. The capillary instability is in particular appreciable in small-scale flow environments. A sketch of the mechanism is shown in Fig. 2. According to the Young–Laplace equation that describes the force balance between the fluid pressure and surface tension on the interface, the surface tension works with the interfacial curvature whose circumferential component destabilizes (i.e., causes interface growth) and longitudinal component stabilizes. Basically, the capillary instability can prevail when the annular layer is more viscous unless the flow is sufficiently fast.

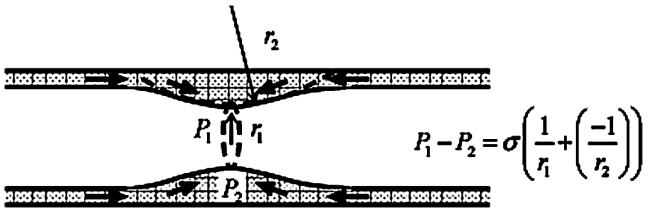

Fig. 2. A sketch of capillary instability in a CAFF. The instability arises from the presence of the circumferential curvature of the interface.

The instability, however, can be arrested by nonlinear effects [9–11], leading to an intact CAFF.

The aforementioned stability analyses of CAFFs are based on steady base flows and are well understood. However, time-periodic base flows could change the stability features of a CAFF. Coward et al. [12] investigated the stability of a pulsatile CAFF. The resulting leading order linear growth rate, similar to the steady or stationary base state case, is attributed to capillarity and is independent of the base flow. They also found that the growth of the instability could be restrained by nonlinear effects. Halpern and Grotberg [13] recently studied the interfacial stability in a liquid-lined tube subject to an oscillatory flow. They showed that sufficiently high frequency could saturate the capillary instability. The mechanism is analogous to a “butter-knife” action in which a growing interface could be suppressed by the shear through the back-and-forth stroke of the airflow. In addition, from the viewpoint of hydrodynamic stability, a certain class of planar Rayleigh–Taylor flow systems shares some similarities with those of CAFFs [14].

Most of the earlier investigations on the effects of surfactants on the interfacial stability of CAFF’s were devoted to the case without a base flow. Halpern and Grotberg [4] and Otis et al. [5] developed lubrication theory models to examine the instability of a surfactant-laden liquid lining that occurs in airway closure. They showed that surfactants prolong closure times because of the Marangoni retardation on the capillary instability. This has been experimentally verified by Cassidy et al. [15]. In particular, for sufficiently high surfactant activity, the interface becomes rigid and the resulting growth rate is reduced to one-fourth of that of the clean interface. The mechanism of the Marangoni retardation of the capillary instability has been explained by Otis et al. [5]. As the capillary instability occurs, the annular fluid is drained from the thinner to the thicker portions of the layer due to capillary pressure differences. Such capillary flow sweeps surfactant likewise, and causes a higher surfactant concentration on the thicker-portion interface, which in turn creates Marangoni forces opposing the capillary growth of the interface.

There are only a few investigations that address how steady base flows influence the surfactant-induced Marangoni effect. Frenkel and Halpern [16] and Halpern and Frenkel [17] studied the linear stability of a two-layer Couette–Poiseuille flow in the presence of an insoluble surfactant. Their analysis showed that surfactant could desta-

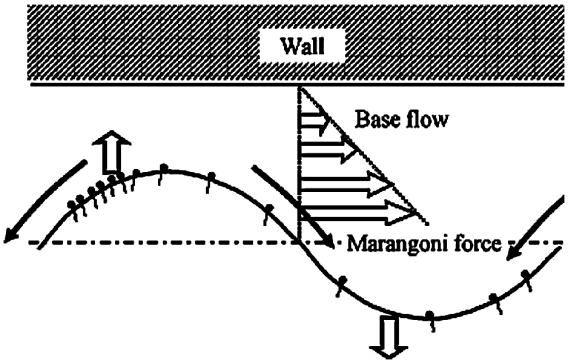

Fig. 3. A sketch of the flow-induced Marangoni instability. A base flow rearranges the surfactant distribution through a varying surface velocity along the deformed interface. The induced Marangoni forces in turn cause the growth of the interface.

bilize the system that is stable in the absence of surfactant. Blyth and Pozrikidis [18] later demonstrated that the Marangoni-induced instability could be arrested by nonlinear effects. Although these studies have addressed how base flows interact with Marangoni effects to affect the interfacial stability, they focus on planar systems that inherently lack the interfacial circumferential curvature that is critical to the capillary destabilization of cylindrical interfaces.

The incorporation of the capillary destabilization in the presence of surfactant has been recently investigated by Wei and Rumschitzki [19]. They asymptotically examined the effect of surfactant on the linear stability of a CAFF. The features of the stability strongly depend on the capillary number Ca, which represents the ratio of viscous to surface tension forces. In particular, in the limit of large Ca, the Marangoni effect destabilizes disturbances for all wavelengths. That is, even when the capillarity effect is absent, the system becomes unstable due to the presence of surfactant. For moderately small Ca, surfactant could cause more severe destabilization than capillarity does.

As illustrated by Wei and Rumschitzki [19], the flow-induced Marangoni instability can be understood by observing the dynamics in the thin-annular region that normally controls the stability of a CAFF. The mechanism is depicted in Fig. 3. The steady base flow in this region behaves like a shear flow that varies linearly in the radial direction. This shear flow basically rearranges the surfactant distribution through a varying surface velocity along the deformed interface. The induced Marangoni forces in turn cause the growth of the interface. A similar mechanism is also present in two-fluid channel flows [16–18].

When a base flow is time-periodic, it is not clear, however, how it modifies the stability features of a surfactant-laden CAFF. In Section 2, we begin with the governing equations, boundary conditions as well as the base state. In Section 3, we utilize scaling analysis to derive a coupled set of evolution equations governing the corresponding linear stability. Results and discussion are presented in Section 4, applications are discussed in Section 5, and conclusions and final remarks are made in Section 6.

2. Base state, governing equations, and boundary conditions

Consider the axisymmetric flow of two immiscible, viscous, incompressible fluids in a core–annular arrangement in a straight tube with radius R_2, as shown in Fig. 1. The interface is given by $r^* = S^*(z^*, t^*)$ where (r^*, θ^*, z^*) are the radial, azimuthal, and axial coordinates used to define a cylindrical geometry. Fluid 1, with viscosity μ_1, occupies the core region $0 \leqslant r^* \leqslant S^*(z, t)$, and fluid 2 having viscosity μ_2 fills the annular region $S^*(z^*, t^*) \leqslant r^* \leqslant R_2$. Our present study is focused on a thin-annular system in which the density stratification does not contribute to the leading-order stability [8]. In the case of a microgravity environment or a higher-than-normal surface tension that occurs in RDS, the gravitational effect could be negligible, similarly in oil recovery. This can be justified based on the magnitude of the Bond number $Bo = \Delta\rho g R_2^2/\sigma^*$ ($\Delta\rho$ the fluid density difference, σ^* the surface tension). For an air–liquid system in RDS occurring in small airways, Bo is about 10^{-2}. During oil recovery in small capillaries, the estimate of Bo is 10^{-3} for a typical water–oil system. For simplicity, the densities of both fluids are assumed to be matched and denoted by ρ. Because the flow fields are assumed to be axisymmetric, the velocity vector is given by $\mathbf{v}^* = (u^*, 0, w^*)$. To study the linear stability of the system, one begins with the unperturbed or base state. Let $r^* = R_1$ be the undisturbed cylindrical interface. The base flow is driven by a time-periodic pressure gradient $\nabla^* p^* = -F(t^*)\underset{\sim}{e}_{z^*}$. In general, this driving force is of the form $F = F_0 + F_1(t^*)$, in which F_0 is the steady part, and the time-oscillatory part F_1 is the time-oscillatory part having frequency ω^*. If the Womersley number $\alpha^2 = \rho\omega R_1^2/\mu_1$ is sufficiently small, then the base flow can be represented by a quasi-steady Poiseuille flow. The base states are given by

$$\mathbf{v}^* = \big(0, 0, \bar{w}^*(r^*, t^*)\big), \qquad [\bar{p}^*] = \frac{\sigma_0^*}{R_1}, \qquad \bar{\Gamma}^* = \Gamma_0^*, \quad (1)$$

where

$$\bar{w}^*(r^*, t^*) = -\frac{F(t^*)}{4\mu_1}\big(r^{*2} - R_1^2\big) + \frac{F(t^*)}{4\mu_2}\big(R_2^2 - R_1^2\big) \quad \text{for } 0 \leqslant r^* \leqslant R_1, \quad (2a)$$

$$\bar{w}^*(r^*, t^*) = \frac{F(t^*)}{4\mu_2}\big(R_2^2 - r^{*2}\big) \quad \text{for } R_1 \leqslant r^* \leqslant R_2. \quad (2b)$$

Here $[\cdot] = (\cdot)_1 - (\cdot)_2$, Γ_0^* is a constant representing the undisturbed surfactant concentration along the undisturbed interface, and σ_0^* is the corresponding interfacial tension. Because we perform a linear stability analysis, we can use a linear relation between σ^* and Γ^*:

$$\sigma^* = \sigma_0^* - \gamma\big(\Gamma - \Gamma_0^*\big), \quad (3)$$

where $\gamma = -(\partial\sigma^*/\partial\Gamma^*)_{\Gamma_0^*}$ is the surfactant elasticity.

Next, the governing equations and boundary conditions are nondimensionalized. We choose R_1 as the characteristic length. The velocity is scaled with respect to the centerline

velocity $W_0 = A_F(R_1^2(\mu_2-\mu_1)+R_2^2\mu_1)/4\mu_1\mu_2$, where the strength of the driving force A_F can be either the steady part $F_0(\neq 0)$, or the amplitude of the oscillatory part F_1 (when $F_0 = 0$). The pressure and time scales are $\mu_1 W_0/R_1$ and R_1/W_0, respectively. The surfactant concentration is scaled with respect to Γ_0^*. The base states (2a) and (2b) then become

$$\bar{W}(r,t) = f(t)\left(1-\frac{mr^2}{(a^2+m-1)}\right) \quad \text{for } 0\leqslant r\leqslant 1, \tag{4a}$$

$$\bar{w}(r,t) = f(t)\left(\frac{a^2-r^2}{a^2+m-1}\right) \quad \text{for } 1\leqslant r\leqslant a, \tag{4b}$$

$$[\bar{p}] = \frac{1}{Ca}, \qquad \bar{\Gamma} = 1, \tag{4c}$$

where $m = \mu_2/\mu_1$ is the viscosity ratio, $a = R_2/R_1$ is the ratio of the tube radius to the unperturbed core radius, $f(t)$ is the dimensionless time-periodic function of the dimensionless frequency $\omega = \omega^* R_1/W_0$ that characterizes the strength of the pressure gradient, and $Ca = \mu_1 W_0/\sigma_0^*$ is the capillary number. The nondimensional equation of state (3) becomes

$$\sigma = 1 - El(\Gamma - 1), \tag{5}$$

where $El = \gamma\Gamma_0^*/\sigma_0^*$ is the elasticity number.

The nondimensional continuity and Navier–Stokes equations for each fluid are

$$\frac{1}{r}(ru)_r + w_z = 0, \tag{6a}$$

$$Re_1(w_t + uw_r + ww_z) = -p_z + m_i\nabla^2 w, \tag{6b}$$

$$Re_1(u_t + uu_r + wu_z) = -p_r + m_i\left(\nabla^2 u - \frac{1}{r^2}u\right), \tag{6c}$$

where

$$\nabla^2 = \frac{\partial^2}{\partial r^2} + \frac{1}{r}\frac{\partial}{\partial r} + \frac{\partial^2}{\partial z^2},$$

and $Re_1 = \rho W_0 R_1/\mu_1$ is the Reynolds number based on the core and $m_i = 1$ and m for $i = 1$ and 2, respectively. Note that $Re_2 = Re_1/m$. At the rigid wall the no-slip and no-penetration-velocity conditions are applied, so that

$$w_2 = u_2 = 0 \quad \text{at } r = a. \tag{7}$$

At the interface $r = S(z,t)$, continuity of velocity, and tangential and normal stress conditions are applied:

$$[w] = 0, \qquad [u] = 0, \tag{8}$$

$$\frac{1}{(1+S_z^2)^{1/2}}\left[(u_z+w_r)\left(1-S_z^2\right)+2(u_r+w_z)S_z\right] = \frac{-El}{Ca}\Gamma_z, \tag{9}$$

$$-\left[p-2u_r-(-p+2w_z)S_z^2+2(u_z+w_r)S_z\right] = \frac{\sigma(\Gamma)}{Ca}\left[S_{zz}-\frac{1}{S}\left(1+S_z^2\right)\right]\left(1+S_z^2\right)^{-3/2}, \tag{10}$$

where $\sigma(\Gamma)$ is given by (5). The kinematic condition, in either core or film variables, is

$$u = S_t + wS_z \quad \text{on } r = S(z,t). \tag{11}$$

Finally, the surfactant transport equation for an insoluble surfactant along the interface [20,21] is

$$\Gamma_t - \frac{S_t S_z}{1+S_z^2}\Gamma_z + \frac{1}{S\sqrt{1+S_z^2}}\left(\frac{S(w+uS_z)}{\sqrt{1+S_z^2}}\Gamma\right)_z + \frac{(u-wS_z)}{(1+S_z^2)^2}\left(\frac{1+S_z^2}{S}-S_{zz}\right)\Gamma = 0. \tag{12}$$

Here we neglect the effects of surface diffusion since the estimated Peclet number $Pe = W_0 R_1/D_s$ (D_s the surface diffusivity) is 10^3 or larger for applications of our interest.

3. Scaling analysis and derivation of evolution equations

Our goal is to asymptotically examine the linear stability of the present system in the thin-film limit. The previous thin-film analysis [8] for a clean-interface CAF has been justified in view of its agreement with the full linear stability analysis [1]. The recent study in a surfactant-laden CAFF [19] also confirmed its consistency with the full analysis based on Stokes flows. We are thus confident that the present asymptotic stability analysis not only captures some of the essential features that should appear in the full stability analysis, but also furnishes a more lucid way to understand the underlying physics prior to performing a complete linear analysis.

We define ε to be the ratio of the undisturbed annular thickness to the core radius. The thin-annulus limit ($\varepsilon \ll 1$) allows one to introduce a stretched film variable $y := 1-(r-1)/\varepsilon$. For $m \sim O(1)$, the base flows (4a) and (4b) to leading order in ε in the annulus and the core are, respectively,

$$\bar{w}(y,t) = \frac{2\varepsilon}{m}f(t)y + O(\varepsilon^2) \tag{13a}$$

and

$$\bar{W}(r,t) = f(t)(1-r^2) + O(\varepsilon). \tag{13b}$$

Let us introduce an infinitesimal axisymmetric disturbance of order δ_1 and δ_2 to the circular interface and the uniform surfactant concentration, respectively,

$$S(z,t) = 1 + \delta_1\eta(z,t), \tag{14a}$$

$$\Gamma(z,t) = 1 + \delta_2 G(z,t), \tag{14b}$$

where η and G are $O(1)$ functions for the interfacial and surfactant concentration perturbations, respectively. Following Wei and Rumschitzki [19], we estimate the scales of perturbation quantities and establish the scaling criterion for capturing both capillary and Marangoni effects in the same leading order. The detailed analysis is outlined in Appendix A.

The required scaling conditions are summarized as

$$Ca \sim \varepsilon^2, \quad El \sim \varepsilon^2, \quad \delta_1 \sim \varepsilon\delta_2. \tag{15}$$

Based on the scalings (15), the scalings of perturbation velocities can be identified. As a result, it can be shown that the leading order stability is governed by the dynamics of the annular film to which those of the core are slaved. We can then derive the corresponding set of evolution equations governing the leading order linear stability of the system. The detailed derivation is provided by Appendix B. As such, letting $Ca_0 = Ca/\varepsilon^2$ and $Ma = El/Ca$, we arrive at the following coupled set of equations:

$$\eta_\tau + \frac{2}{m} f(\tau)\eta_z + \frac{1}{3mCa_0}(\eta_{zz} + \eta_{zzzz}) + \frac{Ma}{2m} G_{zz} = 0, \tag{16a}$$

$$G_\tau + \frac{2}{m} f(\tau) G_z - \frac{2}{m} f(\tau)\eta_z - \frac{1}{2mCa_0}(\eta_{zz} + \eta_{zzzz}) - \frac{Ma}{m} G_{zz} = 0, \tag{16b}$$

where a long time scale $\tau = \varepsilon t$ is necessary for obtaining nontrivial dynamics.

4. Analysis of the leading-order linear stability

We begin with analyzing the leading-order linear stability of the system by considering first the limits of small and large Ma.

4.1. Small and large Marangoni number limits

As $Ma \to 0$, Eq. (16a) reduces to

$$\eta_\tau + \frac{2}{m} f(\tau)\eta_z + \frac{1}{3mCa_0}(\eta_{zz} + \eta_{zzzz}) = 0, \tag{17a}$$

which corresponds to the clean-interface case with a time-periodic base flow. Applying the transform

$$\eta = \hat{\eta} \exp\left(-\frac{2ik}{m} \int f(\tau)\,\mathrm{d}\tau\right) e^{ikz+s\tau},$$

where k is the wavenumber of perturbations and s is the growth rate, we find

$$s = \frac{1}{3mCa_0} k^2(1 - k^2). \tag{17b}$$

As a result, the growth rate s is dominated by capillarity and is independent of the base flow. This is also consistent with the linear stability results of Georgiou et al. [8] and Halpern and Grotberg [13].

In contrast, in the limit of large Ma, the surfactant concentration becomes uniform and the interface becomes tangentially immobile. Such interface, however, still tends to grow due to the capillary instability. Since the tangentially immobile interface retards the flow more than the clean-interface does, the corresponding growth rate should be expected to be slower than the clean interface. In this limit, Eq. (16a) suggests that for $\eta \sim O(1)$, $G \sim 1/Ma$ (i.e., an almost uniform G). By rescaling $G = \tilde{G}/Ma$ with $\tilde{G} = O(1)$, Eqs. (16a) and (16b) can be reduced to

$$\eta_\tau + \frac{1}{m} f(\tau)\eta_z + \frac{1}{12mCa_0}(\eta_{zz} + \eta_{zzzz}) = 0 \tag{18a}$$

at leading order in Ma^{-1}. Using

$$\eta = \hat{\eta} \exp\left(-\frac{ik}{m} \int f(\tau)\,\mathrm{d}\tau\right) e^{ikz+s\tau},$$

the resulting growth rate becomes

$$s = \frac{1}{12mCa_0} k^2(1 - k^2), \tag{18b}$$

which is just one-fourth of that of the clean-interface case (17b) and is again independent of the base flow. This also agrees with the previous studies [15,19]. Notice that the maximum growth rates for both (17b) and (18b) occur at the same wavenumber $k = k_{\max} = 1/\sqrt{2}$.

In general, how the growth rate behaves as Ma varies, e.g., the transition from (17b) to (18b), is not a trivial matter, particularly in the presence of a base flow. The previous study for a steady CAFF [19] showed that the maximum growth rate could be greater or smaller than (17b), depending on the strength of the base flow (reflected by Ca). In the next section we explore the influence of a time-oscillatory base flow in more detail.

4.2. The effect of a time-oscillatory base flow

We choose the function $f(\tau) = \cos(\Omega\tau)$ to characterize a time-oscillatory base flow and examine how such a base flow interacts with surfactant to affect stability. Since Eqs. (16a) and (16b) contain time-dependent coefficients, the usual normal mode analysis is not applicable. We thus utilize Floquet theory and an initial-value-problem approach as alternative solution methods to analyze the features of stability. The details of these methods are given in Appendix C.

According to (C.4) in Appendix C, the system stability is determined by the growth rate s_r, the real part of the Floquet exponent s. Fig. 4 shows the effect of frequency Ω on the linear growth rate s_r as a function of the wave number k. We further confirm that both results using eigenvalue and initial value solution methods are in excellent agreement. Fig. 4 shows that as Ω increases, the growth rate decreases and shifts the critical wavelength $2\pi/k_\mathrm{c}$ toward a larger value, bounded between the small and large Ω limits. In the limit of $\Omega \to 0$, the growth rate approaches that of the steady base flow case with the same flow strength as the maximum of the time-oscillatory one (i.e., $f(\tau) = 1$). On the other hand, in the limit of large Ω, the growth rate approaches that of the stationary base state case (i.e., $f(\tau) = 0$).

To explain the above observations, we should first note that in the presence of surfactant, a steady base flow case

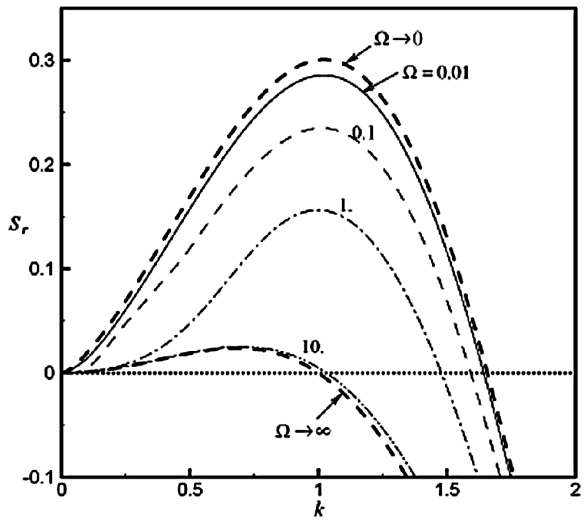

Fig. 4. The effect of frequency Ω on the growth rate s_r as a function of the wave number k. $Ca_0 = 1$, $Ma = 1$, $m = 1$. The base flow is time-oscillatory and has strength of $f(\tau) = \cos(\Omega\tau)$. As $\Omega \to 0$, the growth rate tends to that of a steady-base-flow case with strength $f = 1$. As $\Omega \to \infty$, the growth rate approaches that of the stationary case (i.e., $f = 0$).

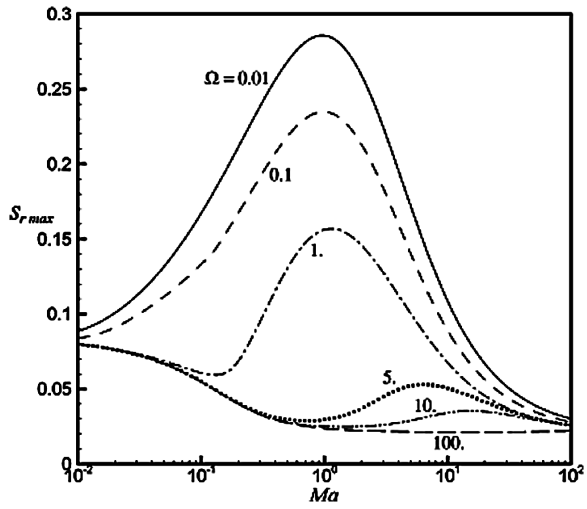

Fig. 5. The effect of frequency Ω on the maximum growth rate $s_{r\,\max}$ as a function of Ma. $Ca_0 = 1$, $m = 1$.The base flow is the same as Fig. 4.

is less stable than a stationary case due to the base-flow-induced Marangoni destabilization [19]. The system becomes less stable as the strength of the base flow increases.

When the base flow is time-oscillatory, disturbances experience time-varying strengths of the base flow in the courses of their evolutions. This suggests that responding growth rates vary between the stationary case (least unstable) and the steady base flow case with the maximum strength (most unstable). When Ω is small, the system could stay with almost unchanged growth rate over a long period of time. During the period when the system has the fastest growth rate corresponding to the maximum base flow strength, the change of the base flow strength is the slowest. The exponential growth of a disturbance thus overwhelms other relatively slower growths during other periods. The smaller Ω becomes, the longer the system can stay with the fastest growth rate. Therefore, in the limit of small Ω, the growth rate approaches the result for the steady base flow case.

For large Ω, the direction of the base flow (with a zero mean) changes rapidly. There is thus no time for surfactant to interact with the base flow to establish a surface tension gradient to cause the Marangoni destabilization. Accordingly, the system with rapidly changing base flow acts in a manner similar to a steady base flow with the same mean. Since the mean of the base flow is zero here, the situation is similar to the stationary case where the capillary instability dominates. In this case, the Marangoni force simply responds to the capillarity and acts as a suppressing force on the capillary instability. In Section 4.3 we will apply the initial value approach with different wave forms for both small and large Ω.

Fig. 5 shows the effect of Ω on the maximum growth rate $s_{r\,\max}$ as a function of Ma for $Ca_0 = 1$. For a given Ma, $s_{r\,\max}$ decreases with increasing Ω just as demonstrated in Fig. 4. For a small Ω (< 1), $s_{r\,\max}$ rises as Ma increases (in the small-Ma regime) and then reaches a maximum at $Ma = Ma^*$ beyond which a further increase in Ma results in a reduction in $s_{r\,\max}$. This is because the base-flow-induced Marangoni destabilization is magnified in the small-Ma regime, while it is suppressed by the less mobile interface in the large-Ma regime [19]. For a large Ω ($\sim$100), however, since the situation should closely follow the case of no base flow, $s_{r\,\max}$ simply declines with increasing Ma. Both trends for small and large Ω suggest that for a moderate Ω, there must be more than one local extremum in the $s_{r\,\max}$–Ma plane, indicating a transition between small- and large-Ω limits. The curves for $\Omega = 1$, 5, and 10 in Fig. 5 illustrate such situations. Further notice that for small and large Ma, all the curves approach the maxima of (17b) and (18b) or the limits $Ma \to 0$ and $Ma \to \infty$, respectively, which are independent of Ω.

The impact of Ω on the maximum growth rate $s_{r\,\max}$ as a function of Ca_0 is shown in Fig. 6. For a small Ca_0 (<0.1), all curves for various Ω merge into a single curve. We identify such a curve as the asymptote $1/12Ca_0^{-1}$, which is just the maximum of (17b) for the clean-interface limit. This is because for a small Ca_0, the system behaves like the stationary case where the capillarity dominates the instability. The base flow thus does not have a significant impact on the instability regardless of Ω. In addition, the Marangoni correction to the leading-order growth rate of $O(Ca_0^{-1})$ is $O(MaCa_0^0)$, which is small compared to the leading order. Obviously, in this small-Ca_0 regime, the maximum growth rate decreases with increasing Ca_0.

Fig. 6 also shows that as Ca_0 increases beyond the small-Ca_0 regime, the effect of Ω on $s_{r\,\max}$ starts to manifest. Again, for a fixed Ca_0 (and Ma), $s_{r\,\max}$ decreases with increasing Ω (see also Fig. 4). For each given Ω, the curve has a minimum at $Ca_0 = Ca_0^*$, beyond which $s_{r\,\max}$ starts to rise as Ca_0 increases. This is because the Marangoni destabilization due to the base flow becomes more pronounced at

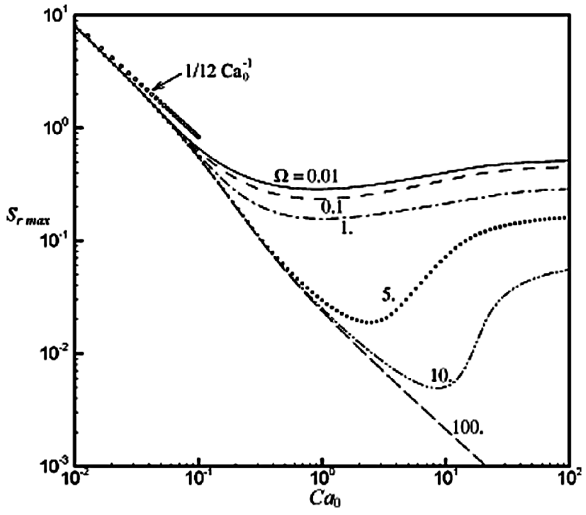

Fig. 6. The effect of frequency Ω on the maximum growth rate $s_{r\,\max}$ as a function of Ca_0, where $Ma = 1$, $m = 1$, and with the same base flow as Fig. 4. As $Ca_0 \to 0$, $s_{r\,\max}$ tends to the rigid-interface limit $1/12\ Ca_0^{-1}$.

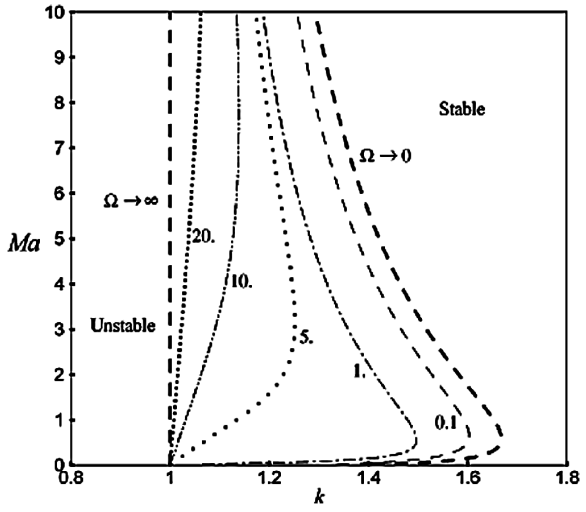

Fig. 7. The effect of frequency Ω on the neutral stability curves in the Ma–k plane. Here $Ca_0 = 1$, $m = 1$, and the base flow is the same as Fig. 2.

larger Ca_0 (since the relative strength of the base flow to capillarity, reflected by Ca_0, becomes larger). Since at higher Ω surfactant has less time to interact with the base flow to generate the Marangoni destabilization, a larger Ca_0^* is needed at higher Ω. It is thus evident that in the large-Ω limit, Ca_0^* tends to infinity (e.g., see the $\Omega = 100$ curve).

Fig. 7 shows the effect of Ω on the neutral stability curves in the Ma–k plane. In conjunction with Fig. 4, increasing Ω shifts the neutral stability curve toward a longer critical wavelength (smaller critical wave number k_c) and shrinks the unstable region. A typical curve has a turning point beyond which a further increase in Ma results in a decrease of k_c. Such a turning point occurs at larger Ma for higher Ω since the capillary instability becomes more dominant at higher Ω so that a larger Ma is required to generate an effective Marangoni destabilization. When Ma is sufficiently large, all the curves for various Ω gradually approach the $k = 1$ asymptote. This is because in the large-Ma limit the growth rate follows (18b), which has $k_c = 1$ regardless of the base flow.

4.3. The effects of different wave forms

So far, the results and discussions are based on the base flow whose strength varies sinusoidally with time with a single frequency. During the normal pattern of breathing, the ratio of the inspiratory time required for a tidal volume to be delivered to the expiratory time before the next breath (i.e., the I:E ratio) is 1:2. Normally, the inspiratory time also includes a pause. For simple sinusoidal waveforms, we find that the growth of the instability is not significantly affected when the I:E ratio is changed from 1:1 to the normal value of 1:2 (not shown). This is because for these waveforms the first-harmonics frequency dominates; the higher frequency contributions to the growth rates are less significant. To further elucidate the effect of I:E by making higher frequency contributions more important, we chose a simple rectangular wave form. This choice is also motivated to test the hypothesis that the longer the system stays at the maximum strength of the base flow, the less stable the system is on average.

The functional form of the rectangular wave having a zero time average is given by

$$f(\tau) = \begin{cases} 0, & \text{if } 0 < \tau < \tau_1 \text{ and } \tau_1 + \tau_2 < \tau < 2\tau_1 + \tau_2, \\ 1, & \text{if } \tau_1 < \tau < \tau_1 + \tau_2, \\ -1, & \text{if } 2\tau_1 + \tau_2 < \tau < T, \end{cases} \tag{19}$$

where $2\tau_1$ denotes the time during a cycle $T = 2\pi/\Omega = 2(\tau_1 + \tau_2)$ when the strength function is turned off, and $2\tau_2$ denotes the remainder of the time during the cycle when the amplitude of the strength function is unity. In Fig. 8 we show the impact of different ratios of τ_1 to τ_2 on the growth rate $s_r(k)$ for a case with $\Omega = 1$, $Ca_0 = 10$, $Ma = 1$. For any combination of τ_1 and τ_2 and for some fixed k, the value of s_r is somewhere in between the steady and no-base flow values, just as the purely oscillatory case. At all wavenumbers, s_r for $\tau_1{:}\tau_2 = 1{:}1$ falls below the purely oscillatory case perhaps because of the increased time during which the strength function is switched off over the oscillatory case represented by the sine function. Increasing τ_1 (or decreasing τ_2) results in a reduction of s_r toward the no-base-flow value, while decreasing τ_1 (and hence increasing τ_2) results in an increase of s_r toward the steady base flow value.

For steady base flows or stationary base states, the growth rate is the real part of $\mathrm{d}\eta/\mathrm{d}\tau/\eta$. We define an instantaneous growth rate $\beta(\tau)$ to be this ratio, namely

$$\beta(\tau) = \Re\left[\frac{\mathrm{d}\eta/\mathrm{d}\tau}{\eta}\right]. \tag{20}$$

Fig. 9 shows how $\beta(\tau)$ varies with τ for $Ca_0 = 10$, $Ma = 1$, $k = 2$, $\Omega = 1$, $\tau_1{:}\tau_2 = 2{:}1$. After an initial transient period of time due to the choice of initial conditions, $\beta(\tau)$ oscillates with period Ω, with an amplitude that is greater than the β

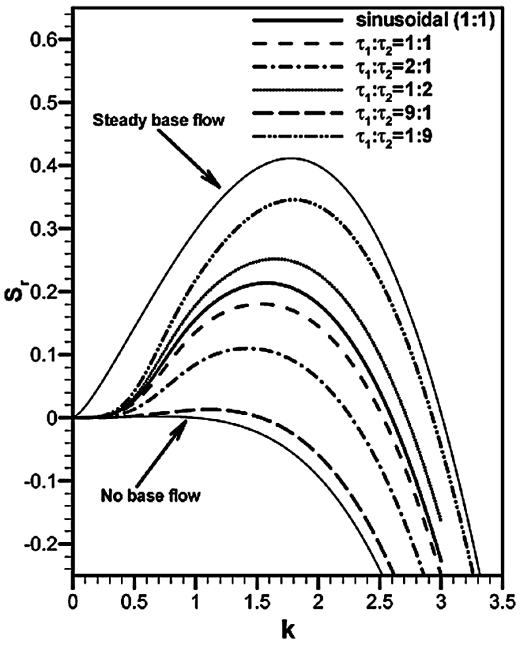

Fig. 8. s_r versus k using a rectangular wave form for the strength of the pressure gradient (Eq. (19)). Here $2\tau_1$ is the time during a cycle $T = 2\pi/\Omega = 2(\tau_1 + \tau_2)$, when the strength function is turned off, and $2\tau_2$ is the rest of the cycle when the amplitude of the strength function is unity. Here $Ca_0 = 10$, $Ma = 1$, $\Omega = 1$.

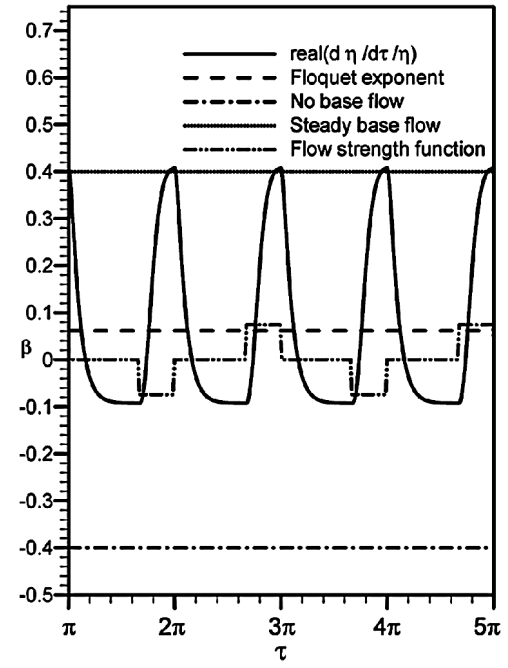

Fig. 9. The instantaneous growth rate β defined by Eq. (20) is plotted as a function of time for $Ca_0 = 10$, $Ma = 1$, $\Omega = 1$, $\tau_1{:}\tau_2 = 2{:}1$, $k = 2$. β lies between the no-base-flow and steady-flow growth rates and has a mean close to the Floquet exponent.

for the no-base-flow case, which is negative for our choice of parameters, but does not exceed the β corresponding to steady base flow. $\beta(\tau)$ increases with τ during the period of time (τ_2) when the strength function is turned on, and keeps on increasing for a short period after the strength function

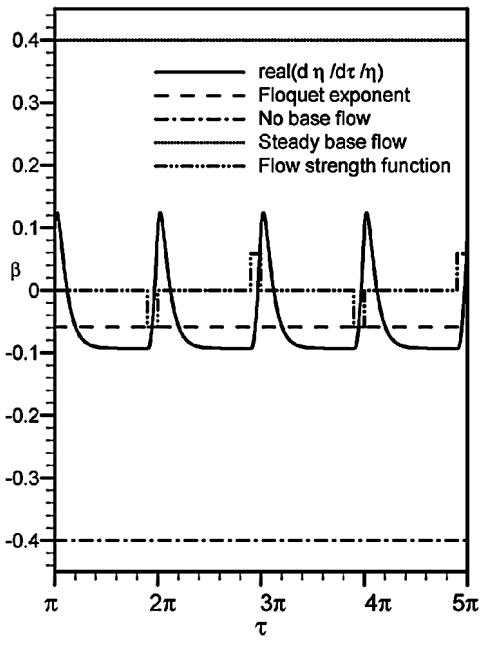

Fig. 10. The effect of increasing the ratio $\tau_1{:}\tau_2$ to 9:1 on the instantaneous growth rate β. In this case, the Floquet exponent is negative, and there are longer periods during which $\beta < 0$ compared to the case shown in figure. This occurs while the strength function is turned off. Also, note that for this particular case, the no-flow and square-wave cases are stable but the steady case is unstable. Here $Ca_0 = 10$, $Ma = 1$, $\Omega = 1$, $k = 2$.

has been turned off before it starts to decrease towards its minimum value. Fig. 10 shows what happens to β if the period of time during which the strength function is turned off is increased, so that $\tau_1{:}\tau_2 = 9{:}1$. The maximum value of β has diminished by approximately a factor of 4 compared to the $\tau_1{:}\tau_2 = 2{:}1$ case, and β remains at its minimum value over a longer period of the cycle. This seems to suggest that the Floquet exponent, which gives a measure of the growth rate over one period of the strength function cycle, has to decrease with increasing τ_1.

4.4. Extension to pulsatile base flows

The above results and discussions are based on a time-oscillatory base flow that has a zero mean. It is also instructive to extend the analysis to a pulsatile base flow that has a steady part modulated with a smaller oscillation, $f(\tau) = 1 + \Delta\cos(\Omega\tau)$, where Δ (< 1) is the oscillation amplitude. We also find that the effect of Ω on the growth rate follows trends similar to those shown in Fig. 4. That is, the growth rate varies between those of the steady base flows having the mean value $f = 1$ (at the high-Ω limit) and the maximum value $f = 1 + \Delta$ (at the low-Ω limit). Since the former (latter) has the slowest (faster) growth rate, this also suggests that the introduction of pulsatility causes more severe destabilization than a steady system. Clearly, for a fixed Ω the growth rate increases with Δ since the strength of the base flow is enhanced. All other stability features are qualitatively similar to those of an oscillatory base flow. We thus do not repeat them here.

5. Application to oil recovery and to the lung

As a typical example of a liquid–liquid displacement, consider an oil film of $\mu_2 = 10$ cP surrounding a water slug ($\mu_1 = 1$ cP) with an interfacial tension of 10 dyn/cm in a 200 μm diameter tube (whose circumference is 628 μm). A typical slug velocity scale is about 1 cm/s [8]. The surface concentration of an insoluble surfactant can range from 10^{-12} to 10^{-10} mol/cm^2 [22]. Consider a film thickness of 10 μm or $\varepsilon = 0.1$. These numbers give $Re_1 \sim 1$, $Ca \sim 10^{-2}$, $m = 10$, and Ma ranging from 2.5 to 250, which is within the range of validity of our analysis. With these parameters, the zero-surfactant-activity limit gives a maximum growth rate of 0.05 min^{-1}, i.e., about a 14-min doubling time. The corresponding wavelength is 888 μm for $k_{\max} = 1/\sqrt{2}$ and the critical wave number is $k_c = 1$. For a steady base flow with a moderate $Ma \sim 2.5$, our theory predicts the maximum growth rate of 0.15 min^{-1}. This growth rate is three times the zero-surfactant-activity case. The corresponding wavelength is 560 μm for $k_{\max} \sim 0.94$. The critical wavelength shifts to a shorter wavelength, 443 μm, for $k_c \sim 1.42$. Introducing a small oscillation into a steady-flow part can modify the above predictions. For example, if the amplitude of the oscillation is 0.2, the same parameters give maximum growth rates varying from 0.15 min^{-1} (high-frequency limit) to 0.18 min^{-1} (low-frequency limit), depending on the frequency. The latter is 1.2 times the former (the steady case). The corresponding wavelength ranges from 587 μm ($k_{\max} \sim 1.07$) to 668 μm ($k_{\max} \sim 0.94$). The critical wavelength also shifts from 361 μm ($k_c \sim 1.74$) to 443 μm ($k_c \sim 1.42$).

For large $Ma \sim 250$, the predicted maximum growth rate should be one-fourth of that of the zero-surfactant-activity case, and is 0.0125 min^{-1}. It is independent of the base flow and is relatively stable compared to the surfactant-free case. The corresponding $k_{\max}$ remains virtually unchanged.

Consider now the liquid lining along the small airways in the lung. At generation 18, the airway diameter is approximately 400 μm [23]. The core fluid here is air ($\mu_1 = 0.02$ cP), and it is assumed that at the distal end of the lung the liquid layer has a viscosity similar to that of water, so that $\mu_2 = 1$ cP. A liquid layer of thickness 5 μm ($\varepsilon = 0.025$) coats the airways. The air–liquid surface tension is 10 dyn/cm in the presence of surfactants. The velocity of air in this small airway is 0.4 cm/s. These give $Re_1 \sim 5 \times 10^{-2}$, $Ca \sim 10^{-5}$, and $m = 50$; thus Ca is clearly small (say, $< O(\varepsilon^2)$), and the system is close to the zero flow limit. The zero-surfactant-activity limit has a maximum growth rate of 0.8 min^{-1}, i.e., about a 0.9-min doubling time. Since the surface tension is much stronger than the strength of the base flow in this case, surfactant tends to stabilize the system (i.e., the Marangoni destabilization is extremely weak) and the critical wave number $k_c \sim 1$. For large Ma, the maximum growth is reduced to 0.2 min^{-1} (one-fourth of the zero-surfactant-activity case).

For liquid plug formation, as in surfactant replacement therapy, consider a slightly larger airway, say at the 10 generation having a diameter of 0.13 cm. The core fluid is still air (0.02 cP) and the annular film has similar properties to water (1 cP). The film thickness is about 10% of the airway diameter, i.e., $\varepsilon = 0.1$. The air–liquid surface tension is 20 dyn/cm when exogenous surfactant is present. For a breathing rate of 30 breaths per minute and a tidal volume of 500 ml, the average air speed in this airway is about 17 cm/s. These conditions give $Re \sim 2 \times 10$, $Ca \sim 10^{-3}$ and $m = 50$. If a surfactant is selected to have property or dosage of $Ma \sim 1$, then the resulting maximum growth rate is 2.2 min^{-1}, which is about five times faster than that of the clean-interface case. Liquid plug formation could be regarded as a result of the interface's snap-off extrapolated from the linear growth at the maximum growth rate. The presence of surfactant thus could potentially promote the formation of liquid plugs. Since the size or length of such a liquid plug can be estimated to be about half of the wavelength occurring at $k_{\max} = 1.5$, the predicted length of a liquid plug is about 0.94 cm, which is shorter than (2/3 of) the periphery of an airway.

6. Concluding remarks

We use scaling and asymptotic analysis to investigate the fate of a CAFF by examining the effects of a time-periodic base flow coupled with Marangoni and capillary forces. In the thin-annulus limit, we derive a set of linear evolution equations coupling the interface with the surfactant concentration that govern the stability of the system. Since these equations have time-periodic coefficients, we employ Floquet theory, or alternatively an initial-value-problem approach, to solve for the linear growth rate of the system, which enables us to investigate the effects of the frequency Ω and different wave forms.

As demonstrated by the previous studies [16,17,19], destabilization can be caused solely by the base-flow-induced Marangoni effect. In particular for CAFF, destabilization could be further reinforced by a combination of both Marangoni and capillary effects. Such destabilization becomes stronger with increasing strength of a base flow. Since a time-periodic base flow has a time-varying flow strength, it could modify the features of such destabilization.

For a time-oscillatory CAFF (having a zero mean), increasing Ω decreases the growth rate and thus stabilizes the system. The maximum growth rate occurs at the limit of small Ω and approaches that of a steady CAFF having the same base flow strength as the maximum of an oscillatory CAFF. In the large-Ω limit, however, the growth rate reaches a minimum corresponding to that of a stationary CAF. Therefore, the introduction of a smaller oscillation into a steady CAFF (i.e., pulsatile CAFF) makes the system more unstable than a steady CAFF. The effects of various wave forms have also been explored and provide further verifica-

tion of our hypotheses for our results at small and large Ω limits.

For the future, it would be interesting to extend the present linear theory into the weakly nonlinear regime to see if the instability can be confined within a small-amplitude regime. In the absence of surfactant, the recent study of Halpern and Grotberg [13] for an oscillatory liquid lining in a tube demonstrated that a sufficiently high frequency could restrain the capillary growth within relatively smaller amplitudes, preventing the snap-off of the core. When surfactant is present, the Marangoni destabilization due to the coupling with the base flow works for all $O(1)$ wavelengths. It is, however, offset by the shortwave capillary stabilization. For a time-periodic base flow, such destabilization also depends on the frequency of the base flow. Therefore, the ultimate fate of the interface would seem to arise from a competition between the Marangoni destabilization, the shortwave capillary stabilization, the flow frequency, and the nonlinear wave steepening to determine whether such a CAFF could retain its integrity.

Acknowledgments

This work was supported by NASA Grants NAG3-2196 and NAG3-2740 and by the National Science Council of Taiwan under Grant NSC92-2218-E006-057.

Appendix A. Scaling analysis

In this appendix, we outline the scaling analysis to estimate the scales of the perturbed quantities. Our strategy essentially follows Wei and Rumschitzki [19]. Let (w'', u'', p'') and (W'', U'', P'') represent the disturbed quantities for the annulus and the core, respectively. The perturbed capillarity furnishes a perturbed annular pressure $p'' \sim \delta_1/Ca$ via the normal stress balance (10). This capillary pressure, via the equations of motion and continuity (6a)–(6c), drives the perturbed film flow and results in the following disturbed velocity scales: $w'' \sim \varepsilon^2\delta_1/Ca$ and $u'' \sim \varepsilon^3\delta_1/Ca$. The velocity scalings of the film demands a long time scale, $\tau = \varepsilon t$, in the kinematic condition (11), so that the interfacial dynamics are nontrivial. A balance of all terms in Eq. (11) leads to $\varepsilon^2\delta_1/Ca \sim \delta_1$, or,

$$Ca \sim \varepsilon^2. \tag{A.1}$$

That is, we are interested in the strong-surface-tension regime. The resulting disturbed annular quantities are $w'' \sim \delta_1$, $u' \sim \varepsilon\delta_1$, and $p'' \sim \delta_1/\varepsilon^2$. For the core quantities, the continuity of the axial velocity across the interface and the lack of a separation of scales determine the perturbed core quantities as $W'' \sim \delta_1$, $U'' \sim \delta_1$, and $P'' \sim \delta_1$. The tangential stress condition (9) now balances the film viscous stress and the Marangoni stress to give $\varepsilon\delta_1/Ca \sim \delta_2 El/Ca$. That is,

$$\delta_2 \sim \delta_1\varepsilon/El. \tag{A.2}$$

If the Marangoni number $Ma = El/Ca \sim O(1)$ or $El \sim \varepsilon^2$, δ_2 is an order of ε lower (i.e., larger) than δ_1 because of $Ca \sim \varepsilon^2$. Thus the surfactant contamination perturbs the annular pressure by an amount $\delta_2 El/Ca \sim \delta_1/\varepsilon$, which is of a higher order in ε than the capillary pressure perturbation $\delta_1/Ca \sim \delta_1/\varepsilon^2$. Note also that the leading-order tangential stress condition (9) now only involves the film quantities, and thus the annular problem is closed without acquiring any information from the core. That is, the annular flow governs the linear interfacial stability and the dynamics of the core are slaved to those of the film.

Finally, we check that (A.2) is consistent with the scaling results from the perturbed surfactant transport equation (12). The leading order of (12) is

$$\varepsilon\delta_2 G_\tau + \bar{w}(1)\delta_2 G_z - \frac{1}{\varepsilon}\bar{w}_y\bigg|_{y=1}\delta_1\eta_z + w''_z = O(\varepsilon\delta_1). \tag{A.3}$$

The first term ($O(\varepsilon\delta_2)$) is the local time rate of change of surfactant concentration, and the other terms all come from the surface convection—the third term of Eq. (12)—in the surfactant balance. The second ($O(\varepsilon\delta_2)$) and fourth ($O(\delta_1)$) terms are the surface convective terms due to the interfacial base flow $\bar{w}(1) = 2\varepsilon f(\tau)/m$ and the perturbation $w'' \sim \varepsilon^2\delta_1/Ca \sim \delta_1$ velocities. The third term, $O(\delta_1)$, arises from the change in the axial velocity of the base flow ($\bar{w} = 2\varepsilon y f(\tau)/m$) evaluated at the perturbed interface. The remaining terms in Eq. (12) are $O(\varepsilon\delta_1)$ or of higher orders. Therefore, the scaling (A.2) is consistent with retaining all of the convective terms in Eq. (A.3), provided that $El \sim \varepsilon^2$ or $Ma \sim O(1)$.

The above scaling is based on the capillary-driven stability mechanism that requires strong interfacial tensions and accommodates Marangoni effects. In fact, the stability can be driven solely by Marangoni effect. This scenario could occur when the capillarity is weak, i.e., $Ca \gg \varepsilon^2$. In this case, the film velocities resulting from the balance with the Marangoni stress are $w' \sim \varepsilon\delta_2 Ma$ and $u' \sim \varepsilon^2\delta_2 Ma$. Inspecting Eq. (A.3) for retaining all relevant terms demands $Ma \sim O(1)$, which is again consistent with that derived from the preceding capillary scaling.

As such, the analysis can be indeed extended beyond the regime of $Ca \sim \varepsilon^2$. In Appendix B, we shall establish the formulation based on $Ca \sim \varepsilon^2$ for capturing both capillary and Marangoni effects in the same leading order. The case of $Ca \gg \varepsilon^2$ can be regarded as the large-Ca limit.

Appendix B. Derivation of evolution equations for the leading order stability

In this appendix, based on the scaling conditions (15), we derive a coupled set of evolution equations for the interfacial

deflection and the surfactant concentration. For the applications of our interest, $Re_1 \sim O(1)$ or less. We postulate the following expansions for the film (small) and core (capital) quantities:

$$w = \bar{w} + \delta_1 w' + O(\varepsilon\delta_1), \qquad u = \varepsilon\delta_1 u' + O(\varepsilon^2\delta_1),$$
$$p = \bar{p} + (\delta_1/\varepsilon^2)p' + O(\delta_1), \tag{B.1}$$
$$W = \bar{W} + \delta_1 W' + O(\varepsilon\delta_1), \qquad U = \delta_1 U' + O(\varepsilon\delta_1),$$
$$P = \bar{P} + \delta_1 P' + O(\varepsilon\delta_1). \tag{B.2}$$

After substitution of (B.1) and (B.2) into Eqs. (6a) and (6b), the governing equations in the annular region become

$$u'_y = w'_z, \qquad 0 = -p'_z + m w'_{yy}, \qquad 0 = -p'_y. \tag{B.3}$$

Using (B.1) and (B.2), and expanding the base state interfacial velocities about their values at the base state interface, we find that the tangential and normal stress balances (9) and (10) become

$$m w'_y = -MaG_z, \tag{B.4}$$

$$p' = \frac{1}{Ca_0}(\eta + \eta_{zz}), \tag{B.5}$$

where $Ca_0 = Ca/\varepsilon^2$ and $Ma = El/Ca$ are $O(1)$. The solution to (B.3) that satisfies the no-slip condition at $y = 0$ and (B.4) is

$$w' = \frac{1}{m}p'_z\left[\frac{1}{2}y^2 - y\right] - \frac{Ma}{m}G_z,$$
$$u' = \frac{1}{m}p'_{zz}\left[\frac{1}{6}y^3 - \frac{1}{2}y^2\right] - \frac{Ma}{2m}G_{zz}y, \tag{B.6}$$

where p' is given by (B.5). The kinematic condition at the interface (11) is

$$u' = \eta_\tau + \frac{2}{m}f(\tau)\eta_z. \tag{B.7}$$

The surfactant transport equation (12) has the same form as (A.3):

$$G_\tau + \frac{2}{m}f(\tau)G_z - \frac{2}{m}f(\tau)\eta_z + \big(w'(y=1)\big)_z = 0, \tag{B.8}$$

where we have invoked a long time scale $\tau = \varepsilon t$ in (B.7) and (B.8) in order to capture all nontrivial evolutions. Substituting of (B.6) with (B.5) into (B.7) and (B.8), we derive the following coupled set of evolution equations given by Eqs. (16a) and (16b):

$$\eta_\tau + \frac{2}{m}f(\tau)\eta_z + \frac{1}{3mCa_0}(\eta_{zz} + \eta_{zzzz}) + \frac{Ma}{2m}G_{zz} = 0,$$
$$G_\tau + \frac{2}{m}f(\tau)G_z - \frac{2}{m}f(\tau)\eta_z - \frac{1}{2mCa_0}(\eta_{zz} + \eta_{zzzz}) - \frac{Ma}{m}G_{zz} = 0.$$

Notice that, as in Georgiou et al. [8], our theory is based on lubrication in the film annulus, which demands that the length scale in the axial direction is much longer than that in the radial direction in the film. Thus predictions of the present theory only hold for $O(1)$ wavelength of a disturbance compared to ε. The theory breaks down when the wavelength is comparable to the thickness of the annulus.

Appendix C. Solution methods

A normal mode analysis cannot be used to determine the growth rate of disturbances since Eqs. (16a) and (16b) contain time-periodic coefficients. In this appendix, we provide alternative solution methods as follows.

C.1. Eigenvalue analysis

One approach to determining the growth rate of the disturbances is to perform an eigenvalue analysis based on Floquet theory. It is more convenient to use the transformation

$$(\eta, G) = \big(\hat{\eta}(\tau), \hat{G}(\tau)\big)\exp\left(-\frac{2ik}{m}\int f(\tau)\,d\tau\right)e^{ikz}, \tag{C.1}$$

where k is the $O(1)$ wavenumber of the disturbances. Substitution of (C.1) into Eqs. (16a) and (16b) yields

$$\hat{\eta}_\tau - \frac{1}{3mCa_0}(k^2 - k^4)\hat{\eta} - \frac{Ma}{2m}k^2\hat{G} = 0, \tag{C.2}$$
$$\hat{G}_\tau - \frac{2ik}{m}f(\tau)\hat{\eta} + \frac{1}{2mCa_0}(k^2 - k^4)\hat{\eta} + \frac{Ma}{m}k^2\hat{G} = 0. \tag{C.3}$$

The transformation (C.1) allows the base interfacial velocity terms $2f(\tau)\eta_z/m$ and $2f(\tau)G_z/m$ to be eliminated in (C.2) and (C.3), respectively. It is also equivalent to the system being in a moving reference frame such that $z' = z - (2/m)\int f(\tau)\,d\tau$. The growth rate does not change since our current system is inertial-free in the film.

We now employ the Floquet theorem to solve Eqs. (C.2) and (C.3), and let

$$\big(\hat{\eta}(\tau), \hat{G}(\tau)\big) = e^{s\tau}\sum_{n=-\infty}^{\infty}(a_n, b_n)e^{in\Omega\tau}, \tag{C.4}$$

where $\Omega = \omega/\varepsilon$ is the dimensionless frequency, and s is an eigenvalue (the Floquet exponent) whose real part s_r determines the growth rate of the system. Also, letting $f(\tau) = \sum_{n=-\infty}^{\infty}\hat{f}_n e^{in\Omega\tau}$, and then substituting (C.4) into (C.2) and (C.3), a set of equations for a_n and b_n is obtained:

$$\left(s + in\Omega - \frac{1}{3Ca_0}(k^2 - k^4)\right)a_n - \frac{Ma}{2}k^2 b_n = 0, \tag{C.5}$$
$$(s + in\Omega + Mak^2)b_n + \frac{1}{2Ca_0}(k^2 - k^4)a_n - \frac{2ik}{m}\sum_{j=-\infty}^{\infty}\hat{f}_j a_{n-j} = 0. \tag{C.6}$$

Equations (C.5) and (C.6) can then be written in a standard matrix form and the eigenvalue is solved subsequently.

C.2. Initial value problem

When the forcing function consists of multiple Fourier modes, it is more convenient to solve an initial value problem for Eqs. (C.5) and (C.6). These equations can be written as

$$\dot{\mathbf{y}} = \mathbf{A}\mathbf{y}, \tag{C.7}$$

where $\mathbf{y} = (\hat{\eta}, \hat{G})$, $\mathbf{A}$ is a 2×2 matrix containing time-periodic coefficients, and the dot denotes differentiation with respect to τ. A 2×2 solution matrix $\mathbf{x}$ is obtained by solving Eq. (C.7) numerically twice over one period $T = 2\pi/\Omega$, such the first column of $\mathbf{x}$ is $\mathbf{y}(T)$ with $\mathbf{y}(0) = (1, 0)$, and the second column of $\mathbf{x}$ is $\mathbf{y}(T)$ with $\mathbf{y}(0) = (0, 1)$. Appealing to the Floquet Theorem, $\mathbf{x}$ satisfies

$$\mathbf{x}(T) = e^{\boldsymbol{\gamma} T}\mathbf{x}(0), \tag{C.8}$$

where $\boldsymbol{\gamma}$ is a 2×2 matrix, which, using (C.7), is determined as follows:

$$e^{\boldsymbol{\gamma} T} = \mathbf{B} = \frac{\mathbf{x}(T) \cdot \mathbf{x}^*(0)}{\mathbf{x}(0) \cdot \mathbf{x}^*(0)}. \tag{C.9}$$

Here $\mathbf{x}^*(0)$ is the complex conjugate of $\mathbf{x}(0)$. The eigenvalues of $\boldsymbol{\gamma}$, which are the Floquet multipliers, can be readily computed once $\mathbf{B}$ is known.

References

[1] L. Preziosi, K. Chen, D.D. Joseph, J. Fluid Mech. 201 (1989) 323.
[2] C.W. Park, G.M. Homsy, J. Fluid Mech. 141 (1984) 257.
[3] J.C. Slattery, AIChE. J. 20 (1974) 1145.
[4] D. Halpern, J.B. Grotberg, J. Biomech. Eng. 115 (1993) 271.
[5] D.R. Otis, J.M. Johnson, T.J. Pedley, R.D. Kamm, J. Appl. Physiol. 75 (1993) 1323.
[6] D.R. Graham, J.J.L. Higdon, J. Fluid Mech. 465 (2002) 213.
[7] L. Rayleigh, Proc. R. Soc. London Ser. A 29 (1879) 71.
[8] E.C. Georgiou, D.T. Papageorgiou, C. Maldarelli, D.S. Rumschitzki, J. Fluid Mech. 243 (1992) 653.
[9] A.L. Frenkel, A.J. Babchin, B.G. Levich, T. Shlang, G.I. Sivashinsky, J. Colloid Interface Sci. 115 (1987) 225.
[10] D.T. Papageorgiou, C. Maldarelli, D.S. Rumschitzki, Phys. Fluids A 2 (1990) 340.
[11] V. Kerchman, J. Fluid Mech. 290 (1995) 131.
[12] A.V. Coward, D.T. Papageorgiou, Y.S. Smyrlis, Z. Angew. Math. Phys. 46 (1995) 1.
[13] D. Halpern, J.B. Grotberg, J. Fluid Mech. (2003).
[14] D. Halpern, A.L. Frenkel, J. Fluid Mech. 446 (2001) 67.
[15] K.J. Cassidy, D. Halpern, B.G. Ressler, J.B. Grotberg, J. Appl. Physiol. 87 (1999) 415.
[16] A.L. Frenkel, D. Halpern, Phys. Fluids 14 (2002) L45.
[17] D. Halpern, A.L. Frenkel, J. Fluid Mech. 485 (2003) 191.
[18] M.G. Blyth, C. Pozrikidis, J. Fluid Mech. 505 (2004) 59.
[19] H.-H. Wei, D. Rumschitzki, submitted for publication.
[20] A.M. Waxman, Stud. Appl. Math. 70 (1984) 63.
[21] H. Wong, D. Rumschitzki, C. Maldarelli, Phys. Fluids 8 (1996) 3203.
[22] K.J. Stebe, S.Y. Lin, C. Maldarelli, Phys. Fluids A 3 (1991) 3.
[23] B. Haefeli-Bleuer, E.R. Weibel, Anat. Rec. 220 (1988) 401.